Piezoelectric, impedance, electric modulus and AC conductivity studies on $(Bi_{0.5}Na_{0.5})_{0.95}Ba_{0.05}TiO_3$ ceramic

Ansu K. Roy, Kamal Prasad, Ashutosh Prasad

University Department of Physics, T.M. Bhagalpur University, Bhagalpur 812007, India

Abstract

Lead-free piezoelectric perovskite ceramic $(Bi_{0.5}Na_{0.5})_{0.95}Ba_{0.05}TiO_3$ (BNT-BT$_{0.05}$), prepared by conventional high temperature solid state reaction technique at 1160 °C/3h in air atmosphere, is investigated by impedance and modulus spectroscopy in a temperature range 35–400 °C, over a frequency range 100 Hz–1 MHz. The crystal structure, microstructure, and piezoelectric properties as well as the AC conductivity of the sample were studied. Powder X-ray diffraction pattern derived from the resulting data at the room temperature subjected to Rietveld refinements and Williamson-Hall plot analysis confirmed the formation of phase pure compound with monoclinic unit cells having a crystallite-size ~33.8 nm. Observed SEM micrograph showed a uniform distribution of grains inside the sample having an average grain size ~3 mm. Longitudinal piezoelectric charge coefficient of the sample poled under a DC electric field of ~ 2.5 kV/mm at 80 °C in a silicone oil bath was found to be equal to 95 pC/N. The frequency and temperature dependent electrical data analysed in the framework of AC conductivity, complex impedance as well as electric modulus formalisms showed negative temperature coefficient of resistance (NTCR) character of the material and the dielectric relaxation in the material to be of non-Debye type. Double power law for the frequency-dependence of AC conductivity and Jump Relaxation Model (JRM) were found to explain successfully the mechanism of charge transport in BNT-BT$_{0.05}$.

***Keywords**: $(Bi_{0.5}Na_{0.5})_{0.95}Ba_{0.05}TiO_3$, morphotropic phase boundary, electrical and piezoelectric properties*

I. Introduction

In view of the recent global concern about the use of eco-unfriendly and hazardous substances in scientific and industry-based devices, the need to reduce environmental contamination by lead-based materials has created a drive to develop alternative lead-free piezoelectric materials. Hence, a large body of work has been reported in the last few decades on the development of lead-free piezoceramics in the quest to replace Lead zirconate titanate (PZT) as the main material for electromechanical devices such as actuators, sensors, and transducers. In specific but narrow ranges of application the new materials appear adequate, but are not yet suited to replace PZT and other lead-based materials on a broader basis from application point of view. $(Bi_{0.5}Na_{0.5})TiO_3$ composition (abbreviated to BNT) discovered by Smolenskii *et al.* in 1960 [1] is one of the important lead-free piezo-

electric materials. As $(Bi_{0.5}Na_{0.5})TiO_3$ composition exhibits a strong ferroelectricity and high Curie temperature T_C ~ 320 °C [2–4], it has been considered to be a good candidate for lead-free piezoelectric ceramics to replace the widely used lead-based piezoelectric materials. It reveals a very interesting anomaly in dielectric properties as a result of low temperature phase transition from the ferroelectric to the anti-ferroelectric phase near 200 °C. However, this material has a drawback of having high conductivity to cause problems in poling process. To improve its properties, some modifications on BNT composition have been performed. It has been reported that BNT-based compositions modified with $BaTiO_3$, $NaNbO_3$, $BiFeO_3$, $Bi_2O_3·Sc_2O_3$ or La_2O_3 [5–10] showed improved piezoelectric properties and easier treatment in poling process compared with those in pure BNT ceramics. Among them, BNT–$BaTiO_3$ (abbreviated to BNT-BT) compositions were more interesting owing to the existence of a [rhombohedral (F_R) / monoclinic (F_M)]-tetragonal (F_T) morphotropic phase boundary (MPB)

* Corresponding author: tel: +91 641 2501699
e-mail: *apd.phy@gmail.com*

around which optimal piezoelectric and ferroelectric performances are often found. Takenaka and other researchers [11–16] also reported that the $(Bi_{0.5}Na_{0.5})_{0.94}Ba_{0.06}TiO_3$ composition near the MPB has relatively high piezoelectric properties. An extensive literature survey revealed that although studies on the dielectric and piezoelectric properties of the BNT-BT$_{0.05}$ and other BNT-BT ceramics have been carried out in the recent years [17–26], no attempt has been made so far to understand the conduction mechanism in BNT-BT$_{0.05}$ ceramic using impedance / modulus spectroscopy technique. Having this in mind, structural, microstructural, piezoelectric, electric impedance / modulus and AC conductivity studies on $(Bi_{0.5}Na_{0.5})_{0.95}Ba_{0.05}TiO_3$ (BNT-BT$_{0.05}$) ceramic, very near MPB composition, have been undertaken in the present work. Also, an attempt has been made to explain the conduction mechanism in BNT-BT$_{0.05}$ using complex impedance and electric modulus spectroscopy techniques and in the light of Jump Relaxation Model for the hopping of charge carriers inside the material.

II. Materials and methods

Polycrystalline $(Bi_{0.5}Na_{0.5})_{0.95}Ba_{0.5}TiO_3$ ceramic was prepared by a standard high-temperature solid-state reaction technique using AR grade (purity more than 99.5%, Hi-Media) oxides and/or carbonates: Bi_2O_3, Na_2CO_3, $BaCO_3$ and TiO_2 in a suitable stoichiometry. The above ingredients were mixed thoroughly, first in air and then in methanol medium, using agate mortar and pestle. This mixture was calcined at an optimized temperature of 1160 °C for about 3 h in an AR-grade covered alumina crucible. Then, by adding a small amount of polyvinyl alcohol (PVA) as binder in the calcined powder, circular and rectangular disc shaped pellets, having thickness in the range of 1–2 mm, were fabricated by applying uniaxial pressure of 6 tons/square inch. The pellets were subsequently sintered at the optimized temperature of 1180 °C in air atmosphere for about 2 h to achieve maximum density (~95% of the theoretical density). The XRD pattern for BNT-BT$_{0.05}$ powder was observed from the data points obtained from an X-ray diffractometer (X'pert-PRO, Pan Analytical, USA), using CuK$_\alpha$ radiation (λ = 1.5405 Å) over a wide range of Bragg angles (20° $\leq 2\theta \leq$ 80°) at the room temperature. The XRD pattern was subjected to the Rietveld refinement for estimating the lattice parameters of the powder sample. The average crystallite size and lattice strain of BNT-BT$_{0.05}$ were estimated using Williamson-Hall approach. Surface morphology of the sintered samples was examined by scanning electron microscope (JEOL-JSM840A). The frequency and temperature dependent dielectric constant (ε_r) and loss tangent (tanδ), complex impedance (Z^*) and phase angle (θ) were measured using a computer-controlled LCR Hi-Tester (HIOKI 3532-50, Japan) on a symmetrical cell

consisting of Ag │ ceramic │ Ag, where Ag is a conductive paint coated on each side of the pellet. Longitudinal piezoelectric charge coefficient (d_{33}) of the poled ceramic sample under an applied DC electric field of about 2.5 kV/mm at 80 °C in a silicone oil bath was measured using a PM3500 d_{33} / d_{31} meter (KCF Technologies, USA).

III. Results and discussion

3.1. Structural study

Figure 1 shows the XRD pattern observed on calcined BNT-BT$_{0.05}$ powder. A standard computer program FullProf.2k (Version 5.30 - Mar2012-ILL JRC) was utilized for the XRD-profile analysis using Rietveld refinements. Good agreement between the observed and calculated inter-planar spacings without any trace of extra peaks due to the constituent oxides suggested the formation of a single-phase compound with monoclinic structure. The evaluated lattice parameters were as follows: a = 8.0829 Å, b = 7.5940 Å and c = 5.8400 Å, β = 109.1787° when indexed in monoclinic system of space group *P2/m* (10). The estimated unit cell volume was ~338.5715 Å^3. All the fitting parameters are reported in Table 1. Figure 2a illustrates the Williamson-Hall plot for BNT-BT$_{0.05}$. The apparent crystallite size and lattice strain are thus estimated to be ~ 33.8 nm and 0.0025, respectively.

3.2. Microstructural study

Figure 2b shows the SEM micrograph of BNT-BT$_{0.05}$ ceramic at magnification of 2500× in which grain shapes are clearly visible, thereby indicating the existence of polycrystalline microstructure. Grains of slightly unequal sizes appear to be distributed throughout the sample. The average grain size was estimated to be ~3 mm. Thus the ratio of grain size to apparent crystallite size in BNT-BT$_{0.05}$ is found to be ~100. Apparent density of the sintered ceramic was found to be ~95% of the theoretical one.
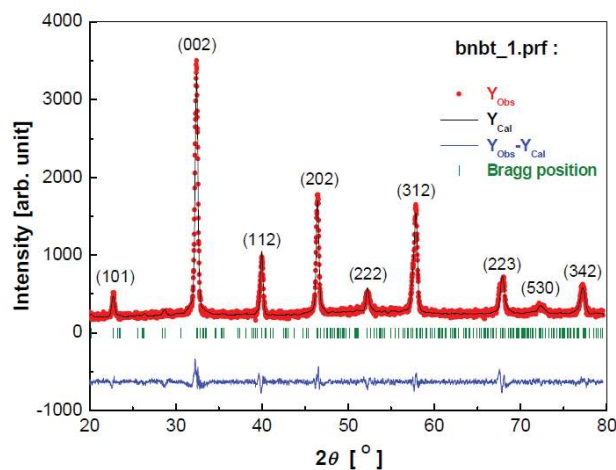

Figure 1. Rietveld refined X-ray diffraction pattern of $(Bi_{0.5}Na_{0.5})_{0.95}Ba_{0.05}TiO_3$ powder at the room temperature

Table 1. The crystal data and refinement factors of $(Bi_{0.5}Na_{0.5})_{0.95}Ba_{0.05}TiO_3$ obtained from X-ray powder diffraction data

Parameters	BNBT05
Crystal system	Monoclinic
Space group	$P2/m$ (10)
a [Å]	8.0829
b [Å]	7.5940
c [Å]	5.8400
β [º]	109.179
V [Å³]	338.5715
R_p	30.8
R_{wp}	23.8
R_{exp}	14.9
R_B	0.873
R_F	1.73
χ^2	2.54
d	0.7661
Q_D	1.8999
S	1.5973

Description of parameters:

R_p (profile factor) = $100[\Sigma|y_i\text{-}y_{ic}|/\Sigma|y_i|]$, where y_i is the observed intensity and y_{ic} is the calculated intensity at the ith step.

R_{wp} (weighted profile factor) = $100[\Sigma\omega_i|y_i\text{-}y_{ic}|^2/\Sigma\omega_i(y_i)^2]^{1/2}$, where $\omega_i = 1/\sigma_i^2$ and σ_i^2 is variance of the observation.

R_{exp} (expected weighted profile factor) = $100[(n\text{-}p)/\Sigma\omega_i(y_i)^2]^{1/2}$, where n and p are the number of profile points and refined parameters, respectively.

R_B (Bragg factor) = $100[\Sigma|I_{obs}\text{-}I_{calc}|/\Sigma|I_{obs}|]$, where I_{obs} is the observed integrated intensity and I_{calc} is the calculated integrated intensity.

R_F (crystallographic R_F factor) = $100[\Sigma|F_{obs}\text{-}F_{calc}|/\Sigma|F_{obs}|]$, where F is the structure factor, $F = \sqrt{(I/L)}$, where L is Lorentz polarization factor.

$\chi^2 = \Sigma\omega_i(y_i\text{-}y_{ic})^2$.

d(Durbin–Watson statistics) = $\Sigma\{[\omega_i(y_i\text{-}y_{ic})\text{-}\omega_{i\text{-}1}(y_{i\text{-}1}\text{-}y_{ic\text{-}1})]^2\}/\Sigma[\omega_i(y_i\text{-}y_{ic})]^2$.

Q_D = expected d.

S (goodness of fit) = (R_{wp}/R_{exp}).

3.3. Piezoelectric study

Longitudinal piezoelectric charge coefficient (d_{33}) of the poled ceramic sample under an applied DC electric field of about 2.5 kV/mm at 80 °C for 15 min in a silicone oil bath was found to be ~95 pC/N.

3.4. Impedance studies

Figures 3a and 3b, respectively, shows the $Z'(f)$ and $Z''(f)$ plots for BNT-BT$_{0.05}$ ceramic at several temperatures between ambient temperature and 450 °C. From the plots it is seen that at lower temperatures Z' decreases monotonically with increasing frequency up to a certain limiting range (~10 kHz) above which it becomes almost frequency independent. The higher values of Z' at lower frequencies and higher temperatures indicate that the polarization in the test material is larger. The temperature at which this frequency-dependent to frequency-independent change of Z' occurs, varies with frequency in the material composition. This also signifies that the resistive grain boundaries become conducting at these temperatures and that the grain boundaries are not relaxing even at the highest measurement ranges of frequency and temperature. $Z''(f)$ plots showed almost identical monotonically decreasing type of variation up to the same frequency limit ~10 kHz beyond
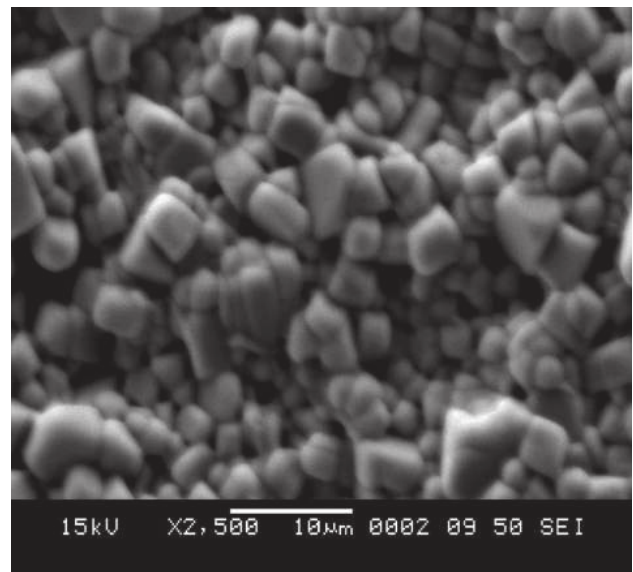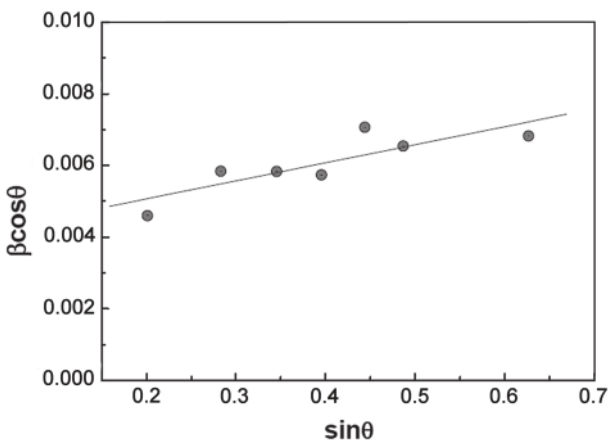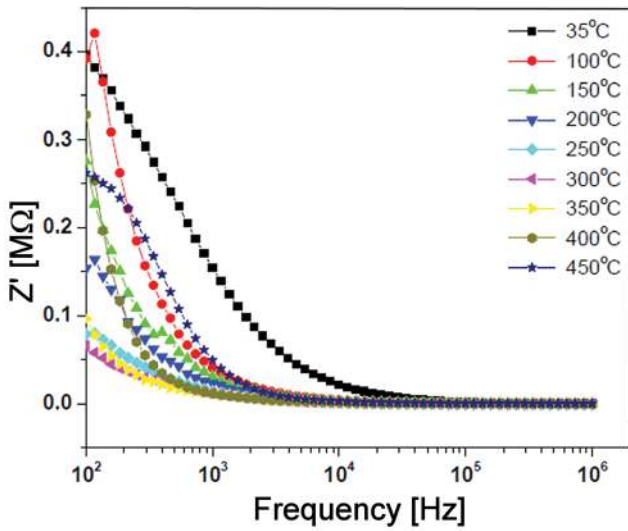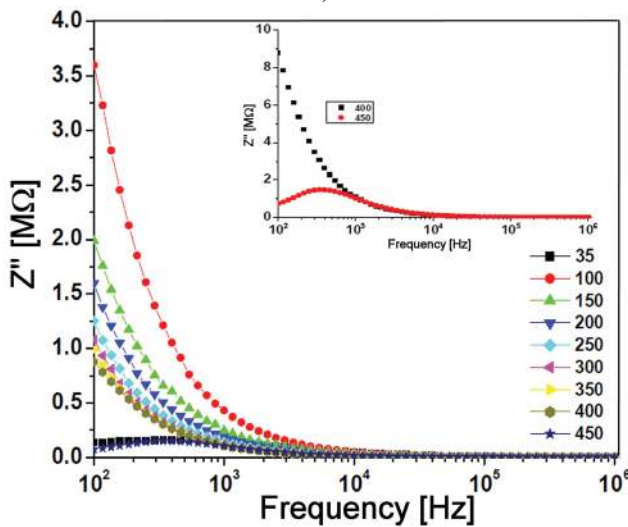

a)

b)

Figure 2. Williamson-Hall plot (a) and SEM micrograph (b) of $(Bi_{0.5}Na_{0.5})_{0.95}Ba_{0.05}TiO_3$ ceramic

**Figure 3: Frequency dependence of: a) *Z'* and b) *Z"*
for(Bi$_{0.5}$Na$_{0.5}$)$_{0.95}$Ba$_{0.05}$TiO$_3$ ceramic at different
temperatures between 35 °C and 450 °C
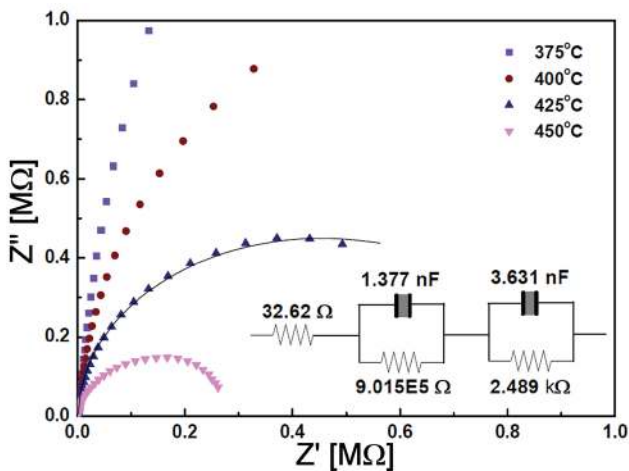*Inset to Fig. 3(b)*: *Z"(f)* plots corresponding to
400 °C and 450 °C**

**Figure 4. Complex impedance plots for
(Bi$_{0.5}$Na$_{0.5}$)$_{0.95}$Ba$_{0.05}$TiO$_3$ ceramic at
different temperatures**

which they merge together at a very low value of *Z"*
to show frequency-independent nature of variation extending up to the highest frequency limit at all the chosen measurement temperatures. The merger of *Z"* (as well as of *Z'*) at higher frequencies for all the temperatures indicates possible release of space charge accumulation at the boundaries of homogeneous phases in the test material under the applied external field. At lower temperatures, monotonic decrease of *Z"* indicated that at lower temperatures the relaxation is absent in the material system. This means that relaxation species are immobile defects and the orientation effects may be associated. Also, the decreasing magnitudes of *Z'* and *Z"* with increasing frequencies implied that relaxation in the material is temperature-dependent, and apparently there is no single relaxation time.

3.5. Complex impedance spectroscopy analysis

Electrical AC data may be presented in any of the four interrelated formalism: relative permittivity $\varepsilon^* = \varepsilon' - j\varepsilon''$; impedance $Z^* = Z' + jZ'' = 1/j\omega C_0\varepsilon^*$; electric modulus $M^* = M' + jM'' = 1/\varepsilon^*$; admittance $Y^* = Y' + jY'' = j\omega C_0\varepsilon^*$; and $\tan\delta = \varepsilon''/\varepsilon' = M''/M' = Z'/Z'' = Y''/Y'$, where $\omega=2\pi f$ is the angular frequency; $C_0 = \varepsilon_0 A/t$ is the geometrical capacitance; $j = \sqrt{-1}$; ε_0 is the permittivity of vacuum (8.854×10^{-12} F/m); t and A are the thickness and area of the pellet; and δ is complementary $(90-\theta)$ to the phase angle (θ), as observed by the LCR Hi-Tester. Complex impedance spectroscopy (CIS) is a relatively powerful method of characterizing many of the electrical properties of materials and their interfaces with electronically conducting electrodes. It may be used to investigate the dynamics of bound or mobile charges in the bulk or interfacial regions of any kind of solid or liquid material: ionic, semiconducting, mixed electronic-ionic and even insulators (dielectrics). An equivalent circuit based on impedance and electric modulus spectra gives an insight into the physical processes occurring inside the sample. Most of the real ceramics contain grains and grain boundary regions, which individually have very different physical properties. These regions are well observed in the impedance and modulus spectra. In polycrystalline materials, impedance formalism emphasizes grain boundary conduction process, while bulk effects on frequency domain dominate in the electric modulus formalism.

The electrical properties of the present material have been investigated using complex impedance spectroscopy (CIS) and complex modulus spectroscopy (CMS) techniques. The Nyquist plots between *Z'(f)* and *Z"(f)* for the BNT-BT$_{0.05}$ ceramic at 375 °C, 400 °C, 425 °C, and 450 °C are shown in Fig. 4. The impedance spectrum is distinguished by semicircles. A series array of two parallel RC combinations (R_g, C_g) and (R_{gb}, C_{gb}) in series with a resistor (R_s) was found to have excellent fits with the experimental data for the test materi-

al, especially at higher temperatures i.e., at 425 °C and 450 °C, thereby indicating the contribution both from grains and grain boundaries of the sample. No other relaxation mechanism such as electrode effect in the sample could be identified through the CIS technique in the studied frequency range. It was observed that at lower temperatures the material showed insulating properties in giving plots in the form of almost straight lines parallel to the ordinate, as shown in Fig. 4. The resulting curves corresponding to higher temperatures showed a tendency to bend towards the abscissa to form semicircles with their centres below the real axis, having comparatively larger radii and the radii decreasing with the increase of temperature, thereby representing the distribution of relaxation times in the test sample and indicating a decrease in the resistivity of the material with the increase in temperature. It thus showed the NTCR and also a clear-cut departure from the ideal Debye type behaviour of the test material. However, the different semicircles from whose radii (R_g, R_{gb}) for the ceramic were evaluated for the ceramic corresponding to the different measurement temperatures have not been shown in the plots, for brevity sake. The Nyquist plot of Z'' vs. Z' corresponding to 425 °C and 450 °C (as shown in Fig. 4) clearly revealed grain and grain-boundary peaks. The data for R_g, R_{gb}, C_g, C_{gb}, τ_g and τ_{gb} are listed in Table 2. Again, the almost frequency-independent data of R_s

are not shown in the Table 2, for brevity sake. The fitted values for R_s, R_g, R_{gb}, C_g, C_{gb} along with an equivalent circuit corresponding to the impedance data for 425 °C have been inserted in Fig. 4. These data yield the grain and grain-boundary relaxation times in the range 1.24 ms – 4.0 µs and 9.037 µs – 0.502 ms at 425 °C and 450 °C, respectively.

3.6. Complex modulus spectroscopic analysis

Complex modulus analysis is an alternative approach to explore electrical properties of the material and to magnify any other effects present in the sample (which are unidentifiable or superimposed on the others in CIS technique) as a result of different relaxation time constants. It is an important and convenient tool to determine, analyse and interpret the dynamical aspects of electrical transport phenomena (i.e. parameters such as carrier/ion hopping rate, conductivity relaxation time, etc.). In order to analyse and interpret the experimental data, it is essential to have a model equivalent circuit that provides a realistic representation of the electrical properties. The modulus representation suppresses the unwanted effects of extrinsic relaxation often used in the analysis of dynamic conductivities of ionically conducting glasses. The dielectric modulus ($M^* = 1/\varepsilon^*$) is frequently used in the analysis of dielectric data of ionic conductors [27–29]. The

Table 2. Grain (bulk)/grain-boundary resistances (R_g/R_{gb}), capacitances (C_g/C_{gb}) and the corresponding relaxation times (t_g/t_{gb}) at the indicated temperatures ranges for $(Bi_{0.5}Na_{0.5})_{0.95}Ba_{0.05}TiO_3$ ceramic

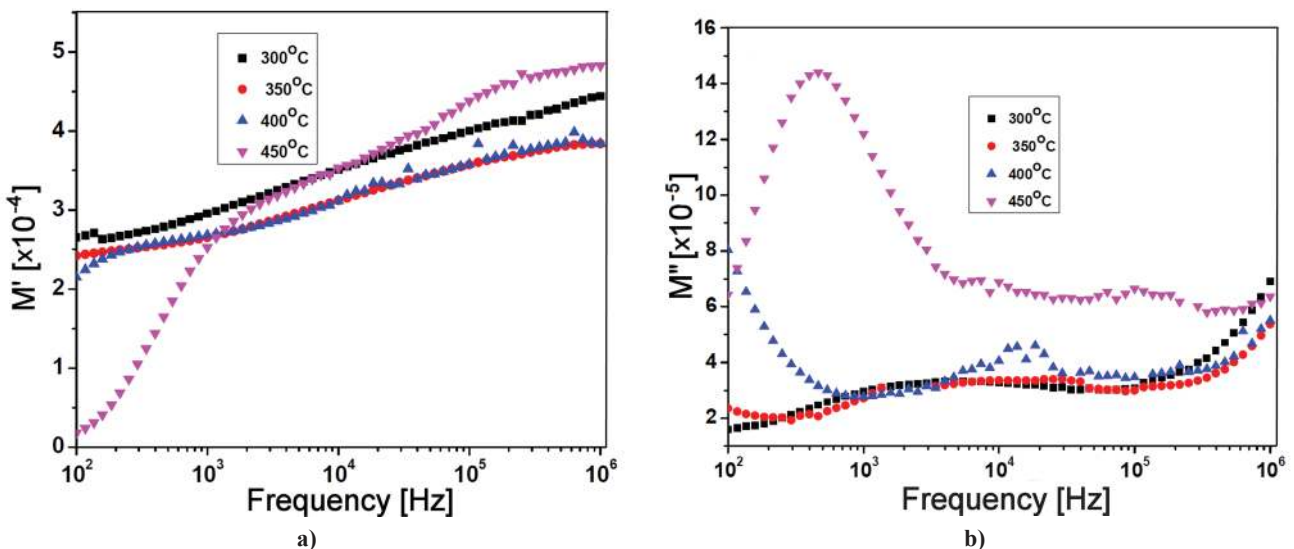| Temperature [°C]	R_g [MΩ]	R_{gb} [kΩ]	C_g [nF]	C_{gb} [nF]	t_g [µs]	t_{gb} [µs]
375	5.61	-	-	-	-	-
400	3.99	-	-	-	-	-
425	0.901	2.489	1.377	3.631	1240	9.037
450	0.163	290	0.0246	1.734	4	502

Figure 5. Frequency dependence of: a) *M'* and b) *M''* for $(Bi_{0.5}Na_{0.5})_{0.95}Ba_{0.05}TiO_3$ ceramic at different temperatures between 300 °C and 450 °C

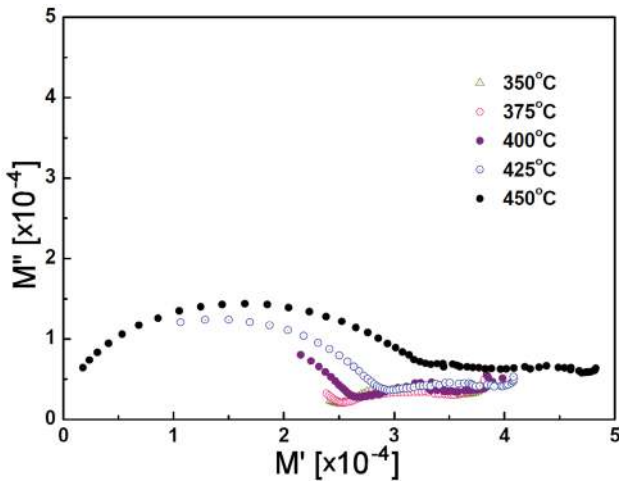**Figure 6. The Nyquist plots in the complex electric modulus plane for $(Bi_{0.5}Na_{0.5})_{0.95}Ba_{0.05}TiO_3$ ceramic corresponding to the data for M' and M'' between 350 °C and 450 °C**

advantage of adopting complex electric modulus spectra is that it can discriminate against electrode polarization and grain boundary conduction processes. Using electric modulus spectroscopic analysis, it is easier to relate this phenomenon to other properties, especially the dynamical mechanical modulus, and the modulus can be written as a single function of conductivity. Sinclair and West [30,31] suggested the combined usage of impedance and modulus spectroscopic plots to rationalize the dielectric properties. Complex impedance plane plots of Z'' versus Z' are useful in determining the dominant resistance of a sample, but are insensitive to the smaller values of resistances. Similarly, complex modulus plots are useful in determining the smallest capacitance. Thus, the power of combined usage of both impedance and modulus spectroscopy is that the Z'' vs. Z' plot highlights the phenomenon of largest resistance whereas M'' vs. M' picks up those of the smallest capacitance [32]. The additional contribu-
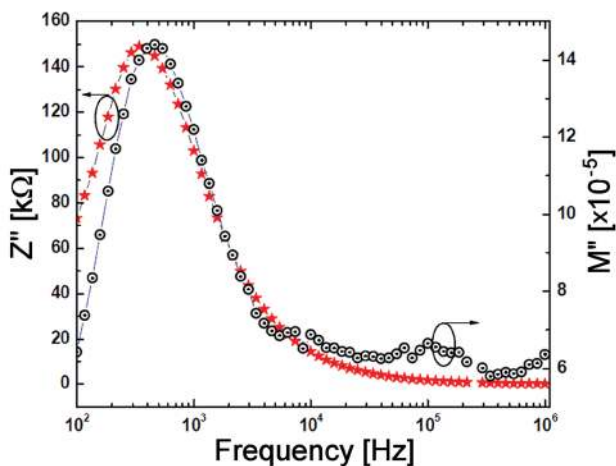
tion in the low frequency part to the specific semicircle is attributed to the blocking effect of the pores. Also, the poor separation of this overlapped semicircle is ascribed to the blocker (pore) size and if the blocker size is greater than 1 µm, it would lead to the overlapping of the semicircles [33]. Figure 5 shows the frequency dependence of: a) real part (M') and b) imaginary part (M'') of complex electric modulus (M^*) for BNT-BT$_{0.05}$ ceramic at different temperatures between 300 °C and 450 °C From the figure it is clear that, at the highest temperature, the $M'(f)$ value tends to zero at low frequencies and shows an almost sigmoid increase with the increase of frequency to reach a maximum (asymptotic value) at high frequencies. Almost similar behaviour is shown for all the $M'(f)$ plots at the chosen temperatures between 300 °C and 450 °C. Such behaviour is an indicative of negligible electrode polarization phenomenon in the test material [34]. The plots of $M''(f)$, as shown in Fig. 5b, exhibit peaks for M'' at different frequencies corresponding to the different measurement temperatures between 300 °C and 450 °C. The frequency region below the peak determines the range in which charge carriers are mobile on long distances. At frequencies above f_{max}, the carriers are mobile on short distances because they are confined to their potential wells. The peaks are also seen to shift to lower frequency side with increasing temperature. The existence of a bit sharper peak at a low frequency (~460 Hz) for the highest measurement temperature i.e., 450 °C suggests that the ions can move over long distances whereas high frequency peaks corresponding to lower measurement temperatures suggest about the confinement of ions in their potential wells. This behaviour suggests that the dielectric relaxation is not the usual thermally activated type in which hopping mechanism of charge carriers dominates intrinsically.

This nature of modulus spectra thus confirms the existence of hopping mechanism in the electrical conduction of the material. The peaks in $M''(f)$ vs. $M'(f)$ plots at the measurement temperatures between 300–450 °C for the test material in the present study suggest that the impedance data can be better analysed by re-plotting them in the modulus formalism. The peak heights are proportional to R for the $Z''(f)$ vs. $Z'(f)$ plots and to C^{-1} for the $M''(f)$ vs. $M'(f)$ plots. The temperature dependence of the complex modulus spectrum (M'' vs. M') of BNT-BT$_{0.05}$ compound is shown in Fig. 6 which clearly indicates the possibility of two semicircles at each of the higher temperatures (from 300 °C to 450 °C) and thus suggests the presence of grain boundaries along with the grains in the test material. Furthermore, at the highest temperature the two semicircles appear clearly separated from each other. At the same time, the radii of the grain-boundary semicircles go on increasing with increasing temperature, thereby showing the mounting dominance of the
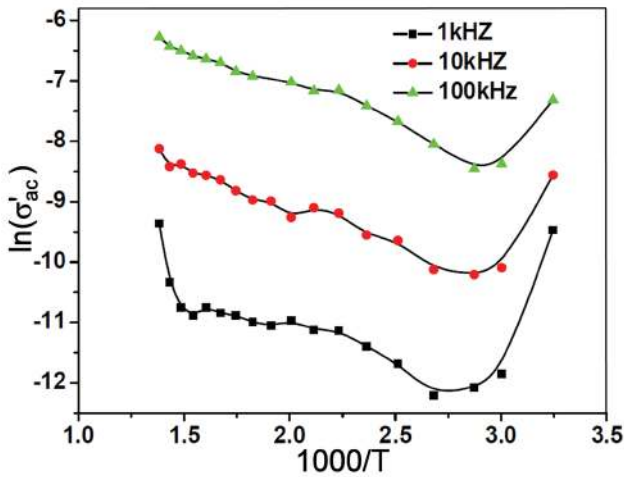

Figure 7. Plots for the imaginary parts of (a) impedance $Z''(f)$ as well as (b) electric modulus $M''(f)$ for $(Bi_{0.5}Na_{0.5})_{0.95}Ba_{0.05}TiO_3$ ceramic corresponding to the experimental data for 450 °C

Figure 8. Dependence of ac conductivity with inverse temperature at the indicated values of frequency for $(Bi_{0.5}Na_{0.5})_{0.95}Ba_{0.05}TiO_3$ ceramic

grain-boundary effect with the increase in temperature and the maximum dominance of grain-boundaries over that of the grains in the given material at the highest measurement temperature. These results indicate the positive temperature coefficient of resistance (PTCR) behaviour of the grain boundaries in BNT-BT$_{0.05}$ ceramic. On increasing the temperature, the intercepts of the right semicircles (corresponding to the grains) on the M'-axis go on increasing. Higher values of M' correspond to higher values of frequencies, as may be seen in the M'–f plots (Fig. 5a), and these higher frequencies correspond to the smaller values of impedance (or resistance), as may be seen in Fig. 3. These results thus indicate the NTCR behaviour for the grains in the test material. These results support the views of Sinclair and West [30,31] that the inner fraction of a grain has semiconducting properties, whereas the grain-boundaries have insulating properties. Figure 7 shows the frequency dependence of the imaginary part of impedance along with that of electric modulus. The region where the peak occurs is an indication of the transition from long-range to short-range relaxation. The overlapping peak positions of $M''_{max}(f)$ and $Z''_{max}(f)$ curves are an evidence of delocalized or long-range relaxation [35], as observed in so many ceramic systems. However, for the present BNT-BT$_{0.05}$ ceramic the M''_{max} and Z''_{max} peaks do not overlap but are close to each other with an appreciable mismatch, thereby suggesting the coexistence of components from both long-range and localized relaxation. In order to mobilize the localized electron, the aid of lattice oscillation is required. Under these circumstances, electrons are considered not to move by their own but by hopping motion activated by lattice oscillation, i.e., by the conduction mechanism. Further, the magnitude of the activation energy endorses the fact that the carrier transport is due to the hopping conduction, as discussed in the foregoing analysis.

3.7. Electrical conductivity analysis

The real part of AC conductivity is given by:

$$\sigma'_{AC} = \omega_i \varepsilon_0 \varepsilon'' \tag{1}$$

where $w = 2\pi \cdot f$, (f being the frequency used); ε_o is the permittivity of vacuum (8.854×10^{-12} F/m) and ε'' is the dielectric loss factor, as referred to earlier. Thus, σ'_{AC} is directly related to the dielectric properties of the material. Alternatively, the real part of the dominant bulk conductivity may be evaluated from the impedance spectrum using the relation $\sigma'_{AC} = t/(Z' \cdot A)$; where Z' is the real part of complex impedance (intersection of semicircle on the real-axis in Z'' vs. Z' plot); t the thickness, and A the surface area of the sample.

Figure 8 shows the plot of the log of AC electrical conductivity (σ_{AC}) versus inverse temperature ($10^3/T$) at three different frequencies (1 kHz, 10 kHz and 100 kHz). It is observed from these plots that in the low temperature regime, AC conductivity increased with increase in frequency, thereby indicating dispersion of conductivity with frequency. With increase in temperature, dispersion in conductivity narrowed down and all the curves for different frequencies appeared to merge at high temperatures, although they did not merge completely even at the highest chosen temperature. The activation energy for conduction was obtained using the Arrhenius relationship:

$$\sigma_{ac} = \sigma_o \exp(-E_a/k_B T) \tag{2a}$$

$$\Rightarrow \ln(\sigma'_{AC}) = \ln(\sigma_o) - E_a/k_B T \tag{2b}$$

Linear least-squares fit to the conductivity data in the above equation 2b gives the value of the apparent activation energy, E_a. The activation energy values for ac conductivity are found to increase with the increase in temperature as shown in Table 3. AC conductivity-based activation energies were calculated at lower frequencies over the higher temperature range (350–450 °C) and they are shown to attain the higher limiting values ~1.431 eV–0.502 eV due to space charge polarization i.e., interfacial effects up to 1 kHz above which the activation energy showed sharp fall to reach a minimum value ~0.079 eV at 100 kHz. In the highest temperature range, the activation energy showed a sudden increase, may possibly be due to the antiferroelectric-to-paraelectric phase change occurring in the material at about 450 °C. This is due to the fact that at low frequencies the overall conductivity is due to the mobility / transportation of charge carriers over long distance rather than from relaxation / orientational mechanism in which case the charge mobility / transportation is restricted only to the nearest neighbouring lattice sites. The enhancement in conductivity with increase in temperature may be considered on the basis that within the bulk, the oxygen vacancies due to the loss of oxygen are usually created during sintering

Table 3. AC/DC conductivity-based activation energies in low and high temperature ranges at different frequencies for $(Bi_{0.5}Na_{0.5})_{0.95}Ba_{0.05}TiO_3$ ceramic

Temperature ranges [°C]	Conductivity-based activation energies [eV] at the indicated frequencies					DC conductivity-based activation energies [eV] at the indicated temperature range
	100 Hz	1 kHz	10 kHz	100 kHz	1 MHz	375–450 °C
350–450	1.431	0.503	-	-	-	1.505
225–450	-	-	0.138	0.079	0.109	-

and the charge compensation follows the Kröger-Vink equation [35]:

$$O_o \rightarrow O_o\!\uparrow + V_o^{\bullet\bullet} + 2e^{-1} \qquad (3)$$
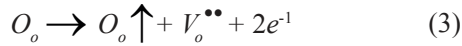
which shows that free electrons are left behind in the process, making the material *n*-type. Further, the merging of the conductivity curves in the higher temperature region results in the release/segregation of space charges, thereby endorsing the results derived from the complex impedance spectroscopic analyses. Approximate values of DC conductivity of the test material were evaluated from the extrapolation of the plateau of the $\sigma_{ac}(f)$ plots up to $f = 0$ corresponding to 375 °C, 400 °C, 425 °C and 450 °C only. Temperature-dependent DC conductivity is given by the following formula:

$$\sigma_{DC} = (\sigma_o/T)\exp(-E_a/k_B T) \qquad (4)$$

from which the slope of the $\ln(\sigma_{DC} \cdot T)$ vs. $10^3/T$ plot yielded the value of activation energy for DC conductivity $E_a = 1.505$ eV, as given in Table 3.

The AC conductivity of the system depends on the dielectric properties and sample capacitance. Figure 9 shows the log-log plot of frequency-dependent AC electrical conductivity (σ_{AC}) at different temperatures. The frequency-dependent conductivity plots of
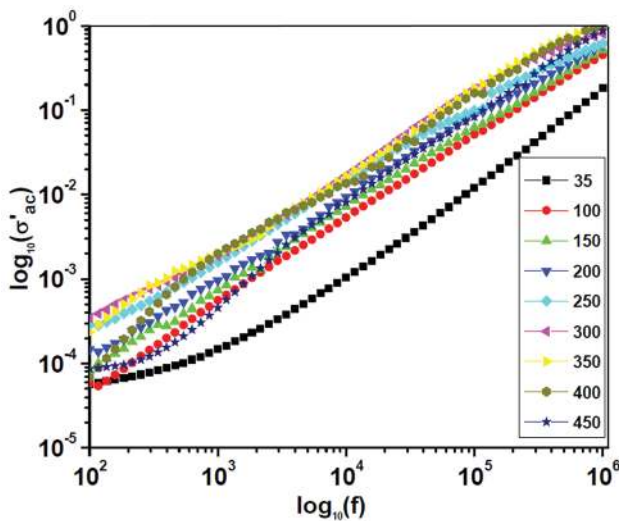

Figure 9. Log-log plot of frequency dependence of real part of complex ac conductivity for $(Bi_{0.5}Na_{0.5})_{0.95}Ba_{0.05}TiO_3$ ceramic at several temperatures between 35 °C and 450 °C

BNT-BT$_{0.05}$ at various temperatures show the spectra which possess a characteristic dispersion displaying the typical shape found for an electronically conducting system. The conductivity spectra have the tendency to merge at higher frequencies with the increase in temperature. At a particular temperature, the conductivity is seen to decrease with decreasing frequency and it becomes independent of frequency after a certain value. The extrapolation of this part towards lower frequency gives σ_{DC} which is attributed to the long range translational motion of the charge carriers. This behaviour may be attributed to the presence of space charge in the material. The basic fact about AC conductivity (σ_{AC}) in BNT-BT$_{0.05}$ is that σ_{AC} is an increasing function of frequency with any type of hopping model taken into account.

The frequency dependence of ac conductivity does not seem to follow the simple Jonscher's power law. On the other hand, it is seen to follow a double power law [37–42] given as:

$$\sigma_{AC} = \sigma_o + A\omega^{s_1} + B\omega^{s_2} \qquad (5)$$

where σ_0 is the frequency independent (electronic or DC) part of AC conductivity. The exponent s_1 $(0 \leq s_1 \leq 1)$ characterizes the low frequency region i.e., it corresponds to the grain-boundary conductivity corresponding to the translational ion hopping, whereas the exponent s_2 $(0 < s_2 < 2)$ characterizes the high frequency region i.e., to the grain conductivity indicating the existence of well localized relaxation/re-orientational process [43], the activation energy of which is ascribed to the reorientation ionic hopping. In the jump relaxation model (JRM) introduced by Funke [38] and extended by Elliot [42] to account for ionic conduction in solids, there is a high probability for a jumping ion to jump back (unsuccessful hop). However, if the neighbourhood becomes relaxed with respect to the ion's position, the ion stays in the new site. The conductivity in the low frequency region is associated with successful hops. Beyond the low frequency region, many hops are unsuccessful and as the frequency increases, there is higher possibility of more hops to be unsuccessful. The change in the ratio of successful to unsuccessful hops results in dispersive conductivity in the test material(s). In the perovskite type oxide materials, the presence of charge traps in the band gap of the insulator is expected. The JRM
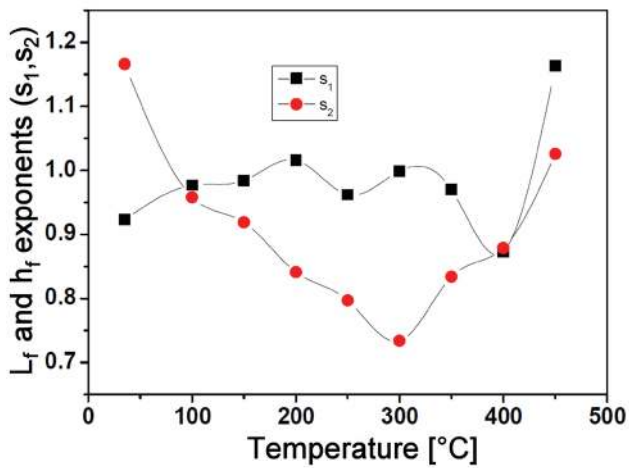
Figure 10. Temperature dependence of low and high frequency exponents (s_1 and s_2, respectively) with temperature for $(Bi_{0.5}Na_{0.5})_{0.95}Ba_{0.05}TiO_3$ ceramic

suggests that different activation energies are associated with unsuccessful and successful hopping processes. The frequency and temperature dependence of AC conductivity in the BNT-BT$_{0.05}$ resembles that of hopping type conduction. Applying JRM to the frequency response of ac conductivity for the test material, experimental conductivity data were found to fit the double power law as given in Equation (5).

Figure 10 shows the temperature-dependent variations of the exponents, (s_1 and s_2) for BNT-BT$_{0.05}$ ceramic between the temperature of ambience and 450 °C. In the present work, s_1 represents the exponent evaluated between the frequency limits of 100 Hz to 54 kHz and s_2 has been evaluated between 60 kHz and 1 MHz. From the plots it is manifested that s_1 assumes maximum values ~0.922 and 1.16 at 35 °C and 450 °C, respectively, while, s_2 assumes maximum values ~1.16 and 1.02 at the same limiting temperatures i.e., at 35 °C and 450 °C, respectively, for the given material. Furthermore, s_1 is seen to assume a minimum value ~0.87 at 400 °C whereas s_2 assumes a minimum value ~0.73 at 300 °C. Due to localization of charge carriers, formation of polarons takes place and the hopping conduction may occur between the nearest neighbouring sites. The nature of conduction has a remarkable relationship with these slopes [44,45]. For small polaron hopping conduction, the value of s increases with temperature, while for large polaron hopping conduction s decreases with temperature [46]. Here, the value of s_1 first increases because of small polaron hopping mechanism [44]. After 300 °C, the slope decreases and reaches a minimum value at 400 °C because of dominant large polaron hopping mechanism (mobility of large polarons is proportional to $T^{-1/2}$). Small polaron formation takes place in those materials whose conduction band belongs to the incomplete "*d*" or "*f*" orbital [44]. In the present case, Ti^{3+} may be assumed to be present in the test ceram-

ic sample due to the reduction of Ti^{4+} into Ti^{3+}, thereby creating incomplete "*d*" orbital, which may possibly be responsible for the small polaron formation. These polaronic states may be thermally dissociated and the residual carriers can form a large polaron due to the interaction with the positive ions in the lattice. The small polaron hopping mechanism is a thermally activated one. Thus as temperature increases, conductivity increases and s_1 increases. But as the temperature exceeds 300 °C, charge carriers trapped in the potential well can form large polarons. These large polarons are easily scattered by the ions and phonons in the material. Thus, the change in conductivity ($\Delta\sigma'_{AC}$) with increase in temperature decreases i.e., s_1 decreases with the increase in temperature. Since the trapped carrier of a large polaron extends over multiple sites, the carrier can continuously adjust to the alternations of the atomic positions and thereby move between sites coherently [47]. Hence, the conductivity increases with the increase in temperature. The value of s_2 has also a decreasing trend with increase in temperature beyond 300 °C. A similar explanation to the temperature-dependent variations of s_2 (as for s_1) also holds good. However, both the frequency exponents s_1 and s_2 are seen to assume their maximum values at 450 °C, thereby showing the dominance of small as well as large polaron hopping in the test material at the ferroelectric-to-paraelectric phase transition temperature i.e., at 450 °C. In the light of the foregoing analysis for the frequency and temperature dependent AC conductivity data for BNT-BT$_{0.05}$ ceramic, the JRM for the hopping of charge carriers may be assumed to hold good in the entire measurement frequency range for the test material composition.

IV. Conclusions

Polycrystalline ceramic sample of $(Bi_{0.5}Na_{0.5})_{0.95}Ba_{0.05}TiO_3$ (BNT-BT$_{0.05}$) was prepared by a conventional high-temperature solid state reaction technique at the sintering temperature of 1180°C. The formation of a single monoclinic phase compound is confirmed by the X-ray diffraction pattern analysis using Rietveld refinement technique. SEM micrograph of the fractured surface of the sintered ceramic pellet shows dense and homogeneous packing and distribution of grains in the material. Longitudinal piezoelectric charge coefficient (d_{33}) of the poled ceramic sample is found to be ~95pC/N. The complex impedance and modulus spectroscopy analyses along with the conductivity studies showed the dielectric relaxation in the material to be of non-Debye type and the overall NTCR character of BNT-BT$_{0.05}$.The study further indicated the contribution of grain-boundaries along with grains in the process of charge transport inside the test material. Activation / binding energies associated with different types of conductivity have also been evaluated.

References

1. G.A. Smolenskii, V.A. Isupov, A.I. Agranovskaya, N.N. Krainik, "New ferroelectrics of complex composition", *Sov. Phys. Solid State*, **2**, (1961) 2651–2664.

2. W.-J. Wu, D.-Q. Xiao, Y. Sun, J.-G. Zhu, J. Li, Z.-J. He; B. Zhang, X.-L. Huang, "Bismuth sodium titanate lead-free piezoelectric ceramics fabricated by using novel low-temperature solid-state synthesis method", *Ferroelectrics*, **404 [1]** (2010) 50–56.

3. A. Sasaki, T. Chiba, Y. Mamiya, E. Otsuki, "Dielectric behavior and microstructure $(Bi_{1/2}Na_{1/2})TiO_3$-$(Bi_{1/2}K_{1/2})TiO_3$-BaTiO$_3$ lead-free piezoelectric ceramics", *Jpn. J. Appl. Phys.*, **38** (1999) 5564–5567.

4. C. Peng, J.F. Li, W. Gong, "Preparation and properties of $(Bi_{1/2}Na_{1/2})TiO_3$-Ba(Ti,Zr)O$_3$ lead-free piezoelectric ceramics", *Mater. Lett.*, **59** (2005) 1576–1580.

5. D.Z. Zhang, Z. Zhenga, X. Feng, T. Zhang, J. Sun, S.H. Dai, L.J. Gong, Y.Q. Gong, L. He, Z. Zhu, J. Huang, X. Xu, "Ferro-piezoelectric properties of $0.94(Na_{0.5}Bi_{0.5})TiO_3$-0.06 BaTiO$_3$ thin film prepared by metal-organic decomposition", *J. Alloys Compd.*, **504** (2010) 129–133.

6. N. Ichinose, K Udagawa, "Piezoelectric properties of $(Bi_{1/2}Na_{1/2})TiO_3$ based ceramics", *Ferroelectrics*, **169** (1995) 317–325.

7. J. Suchanicz, M.G. Gavshin, A.Y. Kudzin, C. Kus, "Dielectric properties of $(Na_{0.5}Bi_{0.5})_{1-x}Me_xTiO_3$ ceramics near orphotropic phase boundary", *J. Mater. Sci.*, **36** [8] (2001) 1981–1985.

8. G.O. Jones, P.A. Thomas, "Investigation of the structure and phase transitions in the novel A-site substituted distorted perovskite compound $Na_{0.5}Bi_{0.5}TiO_3$", *Acta Crystallogr. B*, **58** [2] (2002) 168–178.

9. T. Takenaka, K. Maruyama, K. Sakata, "$(Bi_{1/2}Na_{1/2})TiO_3$-BaTiO$_3$ system for lead-free piezoelectric ceramics", *Jpn. J. Appl. Phys.*, **30** (1991) 2236–2239.

10. Y. Li, W. Chen, J. Zhou, Q. Xu, H. Sun, R. Xu. "Dielectric and piezoelectric properties of lead-free $(Bi_{0.5}Na_{0.5})TiO_3$–NaNbO$_3$ ceramics", *Mater. Sci. Eng. B*, **112** (2004) 5–9.

11. D. Lin, K.W. Kwok, H.L. W. Chan, "Structure and electrical properties of $Bi_{0.5}Na_{0.5}TiO_3$-BaTiO$_3$-$Bi_{0.5}Li_{0.5}TiO_3$ lead-free piezoelectric ceramics", *Solid State Ionics*, **178** (2008) 1930–1937.

12. J-R. Gomah-Pettry, S. Said, P. Marchet, J-P. Mercurio, "Sodium-bismuth titanate based lead-free ferroelectric materials", *J. Eur. Ceram. Soc.*, **24** (2004) 1165–1169.

13. B.J. Chu, D.R. Chen, G.R. Li, Q.R. Yin, "Electrical properties of $Na_{1/2}Bi_{1/2}TiO_3$–BaTiO$_3$ ceramics", *J. Eur. Ceram. Soc.*, **22** (2002) 2115–2121.

14. M. Chen, Q. Xu, B.H. Kim, B.K. Ahu, W. Chen. "Effect of CeO$_2$ addition on structure and electrical properties of $(Na_{0.5}Bi_{0.5})_{0.93}Ba_{0.07}TiO_3$ ceramics prepared by citric method", *Mater. Res. Bull.*, **43** [6] (2008) 1420–1430.

15. R.Z. Zuo, C. Ye, X.S. Fang, J.W. Li, "Tantalum doped $0.94Bi_{0.5}Na_{0.5}TiO_3$-0.06BaTiO$_3$ piezoelectric ceramics", *J. Eur. Ceram. Soc.*, **28** (2008) 871–877.

16. H.-D. Li, C.-D. Feng, W.-L. Yao, "Some effects of different additives on dielectric and piezoelectric properties of $(Bi_{1/2}Na_{1/2})$ TiO$_3$-BaTiO$_3$ morphotropic phase boundary composition", *J. Mater. Lett.*, **58** (2004) 1194–1198.

17. M. Cernea, B.S. Vasile, C. Capiani, A. Ioncea, C. Galassi, "Dielectric and piezoelectric behaviors of NBT-BT$_{0.05}$ processed by sol-gel method", *J. Eur. Ceram. Soc.*, **32** [1] (2012) 133–139.

18. Y. Yao, Y. Yang, S. Ren1, C. Zhou, L. Li, X. Ren, "Ferroelastic and strain glass transition in $(1-x)(Bi_{0.5}Na_{0.5})$ TiO$_3$-xBaTiO$_3$ solid solution", *Europhys. Lett.*, **100** (2012) 17004-p1–5.

19. W. Jo, J.E. Daniels, J.L. Jones, X. Tan, P.A. Thomas, D. Damjanovic, J. Rödel, "Evolving morphotropic phase boundary in lead-free $(Bi_{1/2}Na_{1/2})TiO_3$-BaTiO$_3$ piezoceramics", *J. Appl. Phys.*, **109** (2011) 014110-p1–7.

20. S. Su, R. Zuo, "Fabrication and electrical properties of $0.94Na_{0.5}Bi_{0.5}TiO_3$-0.06BaTiO$_3$ textured ceramics by RTGG method using micrometer sized BaTiO$_3$ plate-like templates", *J. Alloys Compds.*, **525** (2012) 133–136.

21. C. Ma, X. Tan, E. Dulkin, M. Roth, "Domain structure-dielectric property relationship in lead-free $(1-x)$ $Bi_{1/2}Na_{1/2}TiO_3$-xBaTiO$_3$ ceramics", *J. Appl. Phys.*, **108** (2010) 104–105.

22. F. Cordero, F. Craciun, F. Trequattrini, E. Mercadelli, C. Galassi, "Phase transitions and phase diagram of the ferroelectric perovskite $(Na_{0.5}Bi_{0.5})_{1-x}Ba_xTiO_3$ by inelastic and dielectric measurements", *Phys Rev. B*, **81** (2010) 144124 /1–10.

23. C. Ma, X. Tan, "Phase diagram of unpoled lead-free $(1-x)(Bi_{1/2}Na_{1/2})TiO_3$-xBaTiO$_3$ ceramics", *Solid State Commun.*, **150** (2010) 1497–1501.

24. C. Ma, X. Tan, E. Dul'kin, M. Roth, "Domain structure-dielectric property relationship in lead-free $(1-x)$ $(Bi_{1/2}Na_{1/2})TiO_3$-xBaTiO$_3$ ceramics", *J. Appl. Phys.*, **108** (2010) 104105.

25. M. Cernea, L. Trupina, C. Dragoi, B.S. Vasile, R. Trusca, "Structural and piezoelectric characteristics of BNT-BT$_{0.05}$ thin films processed by sol-gel technique", *J. Alloys Compds.*, **515** (2012) 166–170.

26. H.Y. Ma, X.M. Chen, J. Wang, K.T. Huo, H.L. Lian, P. Liu, "Structure, dielectric and ferroelectric properties of $0.92Na_{0.5}Bi_{0.5}TiO_3$-0.06BaTiO$_3$-0.02K$_{0.5}Na_{0.5}NbO_3$ lead-free ceramics: Effect of Co$_2O_3$ additive", *Ceram. Int.*, **39** (2013) 3721–3729.

27. N.G. McCrum, B.E. Read, G. Williams, *Anelastic and Dielectric Effects in Polymeric Solids*, Wiley & Sons, New York, 1967.

28. C.T. Moynihan, "Analysis of electrical relaxation in glasses and melts with large concentrations of mobile ions", *J. Non-Cryst. Solids*, **172-174** (1994) 1395–1407.

29. C.T. Moynihan, L.P. Boesch, N.L. Laberge, "Decay function for the electric field relaxation in vitreous ionic conductors", *Phys. Chem. Glasses*, **14** (1973) 122–125.

30. D.C. Sinclair, A.R. West, "Impedance and modulus spectroscopy of semiconducting BaTiO$_3$ showing positive temperature coefficient of resistance", *J. Appl. Phys.*, **66** (1989) 3850–3856.

31. D.C. Sinclair, A.R. West, "Effect of atmosphere on the PTCR properties of BaTiO$_3$ ceramics", *J. Mater. Sci.*, **29** (1994) 6061–6068.

32. W.S. Warren, K. Vanheusden, D. Dimos, B.A. Tuttle, "Oxygen vacancy motion in perovskite oxides", *J. Am. Ceram. Soc.*, **79** (1996) 536–538.

33. M.J. Forbess, S. Seraji, Y. Wu, C.P. Nguyen, G.Z. Cao, "Dielectric properties of layered perovskite Sr$_{1-x}$A$_x$Bi$_2$Nb$_2$O$_9$ ferroelectrics (A=La, Ca and x=0, 0.1)", *Appl. Phys. Lett.*, **76** (2000) 2934–2936.

34. M. Sural, A. Ghosh. "Electrical conductivity and conductivity relaxation in glasses", *J. Phys. Condensed Matter*, **10** (1998) 10577–10586.

35. A. Chandran, M. Soosen Samuel, J. Koshy, K.C. George, "Dielectric relaxation behavior of CdS nanoparticles and nanowires", *J. Mater. Sci.,* **46** (2011) 4646–4653.

36. F.A. Kröger, H.J. Vink, "Relations between the concentrations of imperfections in crystalline solids", *Solid State Physics*, **3** (1956) 307–435.

37. A.K. Roy, A. Singh, K. Kumari, K. AmarNath, A. Prasad, K. Prasad, "Electrical properties and ac conductivity of (Bi$_{0.5}$Na$_{0.5}$)$_{0.94}$Ba$_{0.06}$TiO$_3$ ceramic", *ISRN Ceramics*, **2012** (2012) 1–10.

38. K. Funke, "Jump relaxation in solid electrolytes", *Prog. Solid State Chem.*, **22** [2] (1993) 111–195.

39. D.P. Almond, C.R. Bowen, "Anomalous power law dispersions in ac conductivity and permittivity shown to be characteristic of microstructural electrical networks", *Phys. Rev. Lett.*, **92** [15] (2004) 5.

40. C.R. Bowen, D.P. Almond, "Modelling the "universal" dielectric response in heterogeneous materials using microstructural electrical networks", *Mater. Sci. Technol.*, **22** (2006) 719–724.

41. G. Bator "Ac and dc conductivity around the ferroelectric phase transition in (CH$_3$NH$_3$)$_3$Bi$_2$Br$_9$ (MABB) crystal", *Ferroelectrics*, **200** [1–4] (1997) 287–295.

42. S.R. Elliot "AC conduction in amorphous chalcogenide and pnictide semiconductors", *Adv. Phys.*, **36** (1987) 135– 217.

43. A. Pelaiz-Barranco, M.P. Gutierrez-Amador, A Huanosta, R. Valenzuela, "Phase transitions in ferrimagnetic and ferroelectric ceramics by ac measurements", *Appl. Phys. Lett.*, **73 [**14**]** (1998) 2039-3.

44. S. Sumi, P. Prabhakar Rao, M. Deepa, P. Koshy, "Electrical conductivity and impedance spectroscopy studies of cerium based aeschynite type semiconducting oxides CeTiMO$_6$ (M=Nb or Ta)", *J. Appl. Phys.*, **108** (2010) 063718–9.

45. M.K. Fayek, S. Mostafa, F. Sayedahmed, S.S. Ata-Allah, M. Kaiser, "On the electrical behavior of nickel ferrite-gallates", *J. Magn. Magn. Mater.*, **210** (2000) 189–195.

46. N. Ortega, A. Kumar, P. Bhattacharya, S.B. Majumdar, R.S. Katiyar, "Impedance spectroscopy of multiferroic PbZr$_x$Ti$_{1-x}$O$_3$/CoFe$_2$O$_4$ layered thin films", *Phys. Rev. B*, **77** (2008) 014111–014120.

47. D. Emin, "Optical properties of large and small polarons and bipolarons", *Phys. Rev. B*, **48** [18] (1993) 13691–13702.